Available online at www.sciencedirect.com
ScienceDirect
Journal of Power Sources 173 (2007) 538–544
JOURNAL OF POWER SOURCES
www.elsevier.com/locate/jpowsour

Phase conversion and morphology evolution during hydrothermal preparation of orthorhombic $LiMnO_2$ nanorods for lithium ion battery application

Qun Liu [a], Dali Mao [a], Chengkang Chang [a,*], Fuqiang Huang [b]

[a] *School of Materials Science and Engineering, Shanghai Jiaotong University, 1954 Huashan Road, Shanghai 200030, PR China*
[b] *Shanghai Institute of Ceramics, Chinese Academy of Sciences, 1295 Dingxi Road, Shanghai 200050, PR China*

Received 1 February 2007; received in revised form 27 March 2007; accepted 29 March 2007
Available online 19 April 2007

Abstract

This paper reports a hydrothermal conversion of MnOOH needles into orthorhombic $LiMnO_2$ nanorods for lithium ion battery application. XRD investigation indicated phase conversion during the Li ion incorporation, and several intermediate phases were formed during the hydrothermal reaction. SEM observation of the sample powder revealed morphological changes during the process, showing that LiOH, not only worked as the Li ion source during the incorporation, but also served as the corrosive media to create nanorod like shape. TEM observation revealed the single crystalline nature of the nanorods and a preferred growth direction along *b* axis direction was also determined. o-$LiMnO_2$ nanorods prepared by such hydrothermal routine showed high electric capacity and stable cyclability at current density of 1/10*C*, indicating potential application in the lithium ion battery field.

Keywords: Hydrothermal; Orthorhombic $LiMnO_2$; Nanorod; Cathode; Capacity

1. Introduction

With the development of electronic technology, demands for portable electronic devices increase quickly. Li-ion secondary batteries as one kind of portable power sources are considered potential candidates in this field, since they own some advantages over the other energy source, such as long cycle life, light weight, low cost and environmental compatibility [1–3]. Commercial applications of batteries based upon $LiCoO_2$ cathode material have been employed in the field since its first commercialization by Sony company in 1990s, with high performances such as high capabilities and elevated-temperature cycling life. However, concerns related to the high cost and environmental toxicity remained as two big drawbacks and required further development within the lithium ion battery system. Recently, lithium manganese oxide compounds attracted researcher's attention for the use as an alterative choice to replace the above-mentioned $LiCoO_2$, since they showed lower cost and better environmental compatibility when compared to the previous cathode material [4–6]. $LiMnO_2$ materials (both in monoclinic and orthorhombic structure), with a high theoretical capacity of 285 mAh g^{-1}, exhibiting a better cyclability even between 2 and 4.5 V versus Li^+/Li, showed a giant potential for industry application among the other lithium manganese oxides.

$LiMnO_2$ cathode material has been studied by many researchers. The monoclinic phase with layered structure was considered very difficult to obtain [7,8], so many works were done with orthorhombic phase (hereafter referred as o-$LiMnO_2$). The o-$LiMnO_2$ phase has been commonly prepared with different methods, such as solid-state reaction at high temperature [9–12], microwave irradiation aided process [13], reverse microemulsion preparation [14] and so on. Recently, electrochemical investigation of o-$LiMnO_2$ showed that the capacity and cyclic behavior are greatly influenced by the synthetic routes and low temperature synthesized o-$LiMnO_2$ offered better properties than the cathode material prepared by solid-state reaction at relatively high temperature. Therefore, some hydrothermal routine that operated at relatively low temperature were developed

* Corresponding author. Tel.: +86 21 62932522; fax: +86 21 62932522.
E-mail address: ckchang@sjtu.edu.cn (C. Chang).

0378-7753/$ – see front matter © 2007 Published by Elsevier B.V.
doi:10.1016/j.jpowsour.2007.03.077

to prepare the material in nanoscale, and related electrochemical properties were reported [15–23]. Among those reports, Mn_2O_3 [15–17] or Mn_3O_4 [18–23] were used as the main Mn ion source which reacts with LiOH solution to form the o-$LiMnO_2$. However, the process how the o-$LiMnO_2$ cathode material was formed during the hydrothermal routine and how to control the growth manner of the nanoscaled crystals have not been reported yet.

In this paper, a hydrothermal reaction was designed to prepare nanorod like o-$LiMnO_2$ using needle like MnOOH as a precursor. The phase conversion and morphological evolution during the hydrothermal reaction were investigated. Electrochemical tests revealed a stable capacity around 150 mAh g^{-1} at current density 0.1*C*, showing potential application of the material in lithium ion battery field.

2. Experimental section

The rod like o-$LiMnO_2$ cathode material was prepared through a two-step hydrothermal routine. All the raw materials employed in the experiment were of analytical grade and not further purified in the experiment. A need like MnOOH was firstly synthesized to serve as precursor for the preparation of the o-$LiMnO_2$ nanorods [24,25]. In a typical process [24], 0.6 g Mn_2O_3, purchased form Aldrich, was added into 30 ml 7% HCl solution, with a continuous stirring for 10 min. Then the solution was transferred into a Teflon linked autoclave and kept at 100 °C for 5 h to dissolve the oxide. When the autoclave was cooled down to room temperature, solid sodium hydroxide was added to the solution to adjust the PH value to ca. 9. The autoclave was sealed again and kept at 180 °C overnight for 20 h. After the autoclave was cooled, a brown precipitate was collected and washed with distilled water three times and finally dried at 60 °C for 20 h. The obtained powder was confirmed to show a MnOOH structure by XRD investigation. o-$LiMnO_2$ nanorods were prepared using the above-mentioned precursor. Six grams of $LiOHH_2O$ was dissolved in 40 ml distilled water, and then 1 g of the MnOOH material was added. After stirring for 10 min, the solution was further ultrasonically treated for 10 min. The above-prepared solution was transferred into an autoclave and kept in an electric oven which was previously set at 200 °C. After different time periods (2, 3 and 4 h), the autoclave was picked out and rapidly cooled down to room temperature in flowing water. The finally obtained precipitates were collected, washed with distilled water and dried at 60 °C.

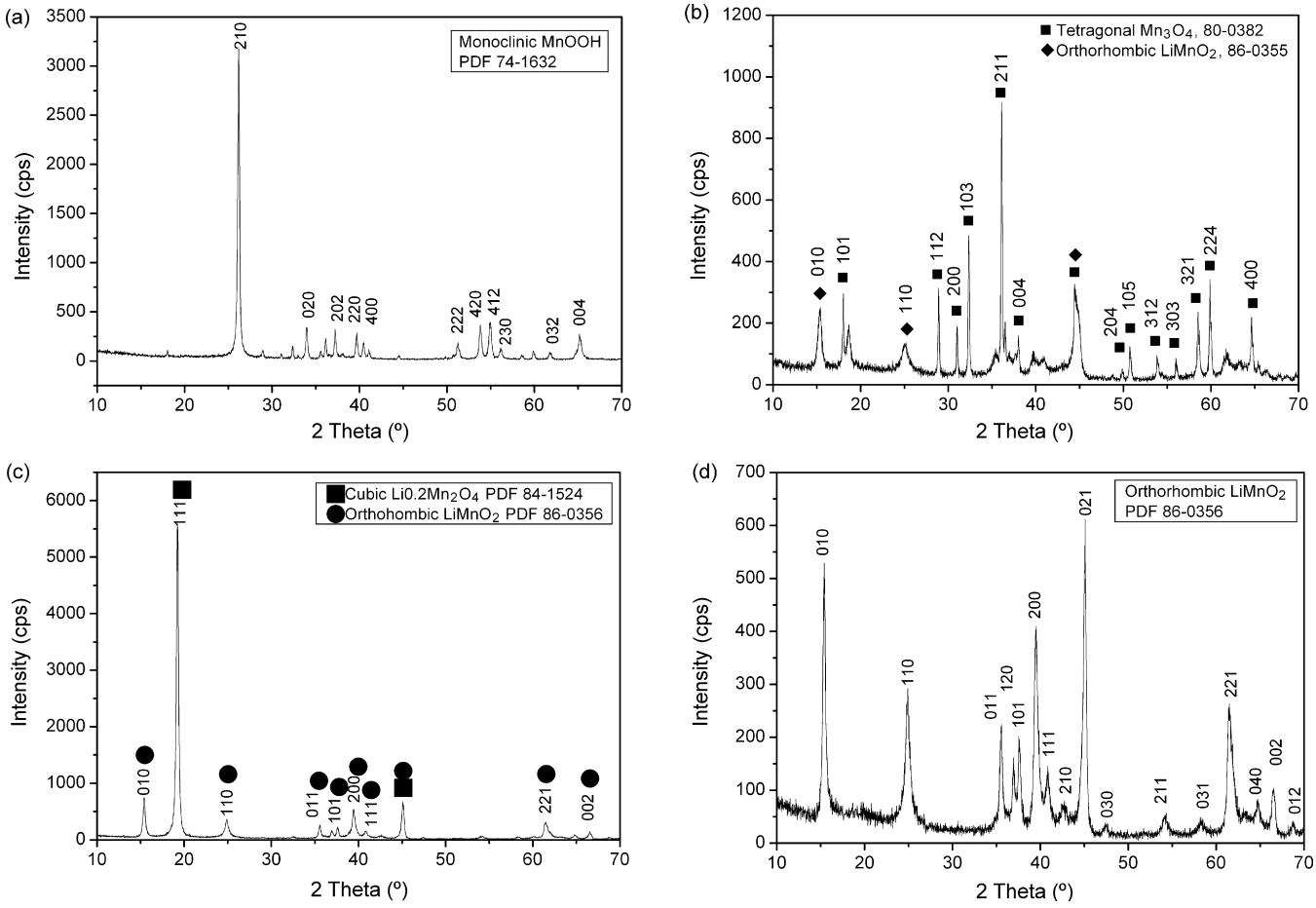

Fig. 1. XRD patterns of the products after hydrothermal treatment under 200 °C for different time period, showing the phase transition during the Li ion incorporation. (a) Original MnOOH precursor with a monoclinic structure, (b) sample obtained after 2 h treatment, showing the intermediate tetragonal Mn_3O_4 phase, (c) sample obtained after 3 h treatment, implying the existence of cubic $Li_{0.2}Mn_2O_4$ phase, and (d) pure o-$LiMnO_2$ after 4 h hydrothermal treatment.

The characterization of the precursor and the obtained powder products were conducted with various methods. Both the MnOOH precursor and the hydrothermally prepared products were examined by means of XRD, SEM and TEM to confirm the phase composition, morphological change and preferred growth direction. X-ray diffraction (XRD) patterns were obtained on a JEOL-JDX3500 X-ray diffractometer employing Cu Kα radiation (1.54178 nm), with a scanning rate of 0.02° per step in the 2θ range from 10° to 70°. The morphologies were observed with a JEOL-JSM-6700 field emission scanning electron microscope (FESEM). TEM observation was carried out with a field emission TEM, Hitachi HF-3000S, equipped with a CCD camera for the image process.

The electrochemical property of the o-$LiMnO_2$ nanorods was evaluated with coin type cell. Cathodes were prepared by mixing the hydrothermally prepared oxide powders, acetylene black, and polyvinylidene fluoride (PVDF) in the weight ratio of 80:10:10 with *N*-methyl pyrrolidone (NMP) served as the solvent. A black slurry was finally obtained, which then was pasted on an aluminum foil and dried for 2 h at 120 °C. The dried foil was transferred to a vacuum oven and kept under 80 °C overnight for further drying. Coin type cell was assembled with the cathode as a working electrode, and lithium foil as a counter electrode in an Ar-filled glove box. The cells were first charged and then discharged between 2.0 and 4.5 V versus metallic Li with a current density of 1/20*C* and 1/10*C* at room temperature.

3. Results and discussion

3.1. Phase transition during the formation of o-$LiMnO_2$

It hade been reported by several research groups that o-$LiMnO_2$ can be obtained using MnOOH and $LiOHH_2O$ as the starting materials [10,26]. However, the process how the o-$LiMnO_2$ phase was formed had not yet been discovered. Recently, Williams [27] reported the kinetic process of the incorporation of Li into MnOOH to form o-$LiMnO_2$ using in situ X-ray and neutron diffraction method, in which a direct reaction between MnOOH and LiOH to form o-$LiMnO_2$ was assumed. However, in our case, some intermediate phases were formed during the Li ion incorporation, implying a complex reaction during the hydrothermal process. A detailed XRD investigation of the samples prepared with different reaction time is shown in Fig. 1. Fig. 1a shows the XRD pattern of the MnOOH precursor, where a very strong reflection peak was observed, beside several weak peaks. Those reflections can be indexed into a

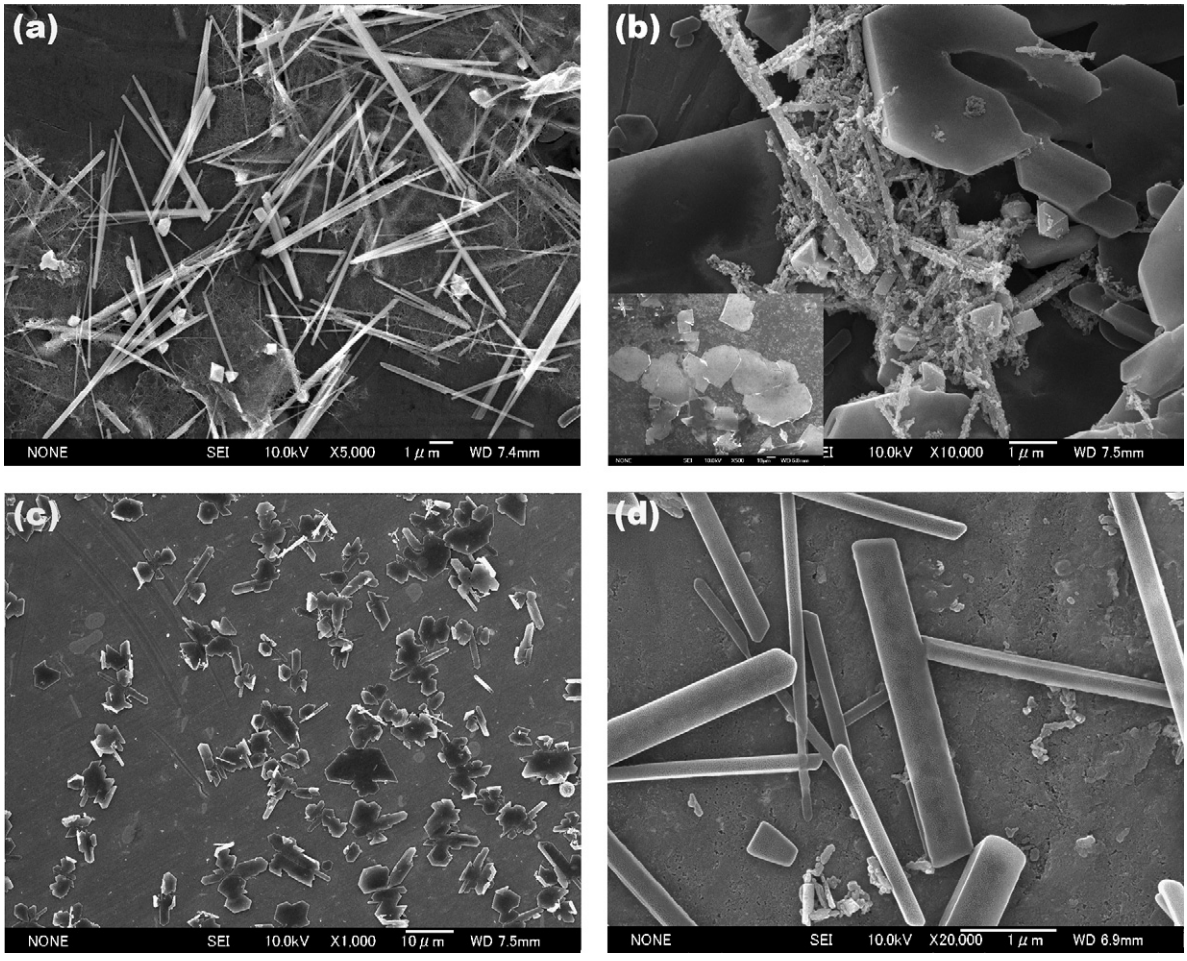

Fig. 2. SEM micrograph of sample powders with different hydrothermal time. (a) The MnOOH precursor, (b) 2 h incorporation, (c) 3 h incorporation, and (d) 4 h incorporation.

monoclinic phase of MnOOH according to standard powder diffraction file PDF 74-1632. After hydrothermally treated in LiOH solution for 2 h, the XRD pattern looked quite different, and the monoclinic MnOOH phase disappeared, as shown in Fig. 2b. A careful investigation into the pattern revealed that the pattern can be indexed into two phases, tetragonal Mn_3O_4 and o-$LiMnO_2$. It can be recognized from the pattern that Mn_3O_4 phase exists in the powder as the main component while the amount of o-$LiMnO_2$ is very small. The formation of Mn_3O_4 implied that a slight reduce of Mn^{3+} ions happened in this stage. After hydrothermal treatment of 3 h, another phase was identified, as can be seen from Fig. 1c. A very strong reflection peaking at 2θ at ca.19.25° was observed, indicating the existence of a lithium deficient lithium manganese oxide phase, a cubic $Li_{0.2}Mn_2O_4$ phase. The formation of such cubic $Li_{0.2}Mn_2O_4$ phase (with Mn valence of 3.9) could be explained by the dissolving of Mn^{2+} from the $Mn^{2+}Mn_2{}^{3+}O_4$ into the LiOH solution [28] according to the mechanism proposed by Myung et al. To keep the valence balance, the Mn^{3+} ions in 8d sites will be oxidized and the valence be increased. According to this mechanism, we presume that after the dissolution of Mn^{2+} ions, Li^+ ions will occupy the 4a sites and therefore results in the formation of $Li_{0.2}Mn_2O_4$ and finally $Li_2Mn_2O_4$ phase will be obtained with further Li^+ ions intercalation. The $Li_2Mn_2O_4$ will later be converted into $LiMnO_2$ phase with further hydrothermal treatment and large amount of o-$LiMnO_2$ appeared after 4 h, as shown in Fig. 1d. All the intermediate phases disappeared, but the o-$LiMnO_2$ phase remained. All the reflections can be indexed to the o-$LiMnO_2$ structure according to PDF 86-0356. The above results strongly indicate that the reaction during Li ion incorporation was much more complicated, phase transition accompanied by the valence change of Mn ion occurred throughout the hydrothermal process. An interesting and important fact is the observation of tetragonal Mn_3O_4 during the hydrothermal process, which indicated that the Mn_3O_4 served as an intermediate phase for the hydrothermal reaction, showing good accordance with the reports by the other groups employing Mn_3O_4 as the precursor [18–21]. A big difference between the MnOOH and Mn_3O_4 routine is the reacting time required to form the o-$LiMnO_2$. In our case, only 4 h are needed to get well crystalline nanocrystals, while 4 days are required in the Mn_3O_4 routine. Although the reason is not clear at present, such big difference suggested that the MnOOH routine has a giant advantage over the Mn_3O_4 routine in the viewpoint of energy saving and thus has great potential in practical application.

3.2. Morphological evolution during the Li ion incorporation

The original purpose of the experiment is to prepare o-$LiMnO_2$ in some special shapes, such as nanowire or nanorod. So we followed Du's method [24] to synthesize rod like MnOOH to serve as an precursor, hoping that the rod like shape will be kept after the Li ion incorporation. Although nanorods were obtained after the hydrothermal reaction, but the forming mechanism is quite different from what we thought before. SEM observation of the sample powders obtained at different hydrothermal time revealed a morphological change during the lithium incorporation. The SEM micrograph of the starting MnOOH precursor shown in Fig. 2a revealed needle like structures, with diameter around several hundred nanometer, length about ten micron. After 2 h incorporation, most of the needle like structures disappeared, and new crystals with platy shape and big size were observed, as shown in the bottom left inset in Fig. 2b. A typical morphological change was also observed in the center of the micrograph, where original needle like MnOOH crystal was observed, with some tiny crystals adhered. Such image strongly implied that the MnOOH needles were corroded by the high concentrated LiOH solution, and the tiny crystals can be regarded as the residual of the original MnOOH precursor which later were converted into Mn_3O_4 crystals with platy shape. After 3 h hydrothermal treatment, all the tiny crystals disappeared, platy structures, with irregular shape, were observed, as shown in Fig. 2c. After 4 h treatment, the platy crystals disappeared again,

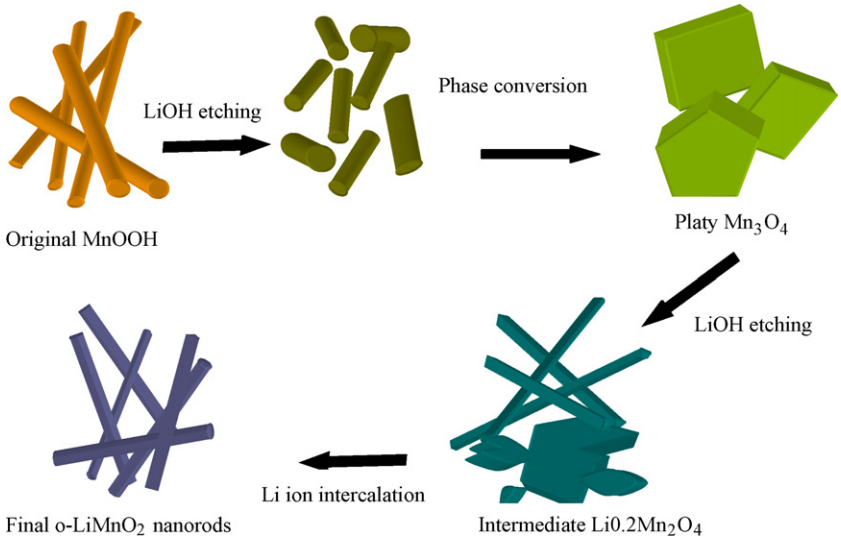

Fig. 3. A scheme showing the formation of o-$LiMnO_2$ nanorod.

rod like o-$LiMnO_2$ crystals, with obvious edges, were observed in Fig. 2d. The above morphological changes during the lithium incorporation greatly indicated that LiOH played two different roles during the process, one as the reaction material to form the final o-$LiMnO_2$, and the other as the corrosive medium which caused the morphological change due to the highly concentrated alkali LiOH solution.

Based on the above XRD investigations and SEM observations, the reaction process during the Li ion incorporation can be summarized, and explained schematically in Fig. 3. In the first step, needle/rod like MnOOH precursors were eroded into tiny particle like crystals, and then those tiny crystals were transferred into platy intermediate tetragonal Mn_3O_4. Only a small amount of the crystals were converted into o-$LiMnO_2$. In a second step, the well intermediate phases was further eroded into small pieces with irregular shape, and lithium ion incorporation took place at the same time and Li deficient $Li_{0.2}Mn_2O_4$ phase was formed. And finally, after the formation of $Li_{0.2}Mn_2O_4$, further Lithium incorporation and corrosion continued and finally pure phased o-$LiMnO_2$ was formed.

3.3. Growth manner of the o-$LiMnO_2$ nanorods

TEM observation of the nanorods are shown in Fig. 4. In Fig. 4a, a single nanorod was presented, with a few fragments adhered on the surface. A high resolution TEM micrograph of the tip of the nanorod is shown in Fig. 4b, from which clear fringes were observed, illustrating the single crystalline nature of the nanorod. The spacing between the two sets of the fringes were measured as 0.592 and 0.281 nm, showing good agreements with lattice planes of (0 1 0) and (0 0 1). A FFT image of Fig. 4b is shown in Fig. 4c, where calculated electron diffraction

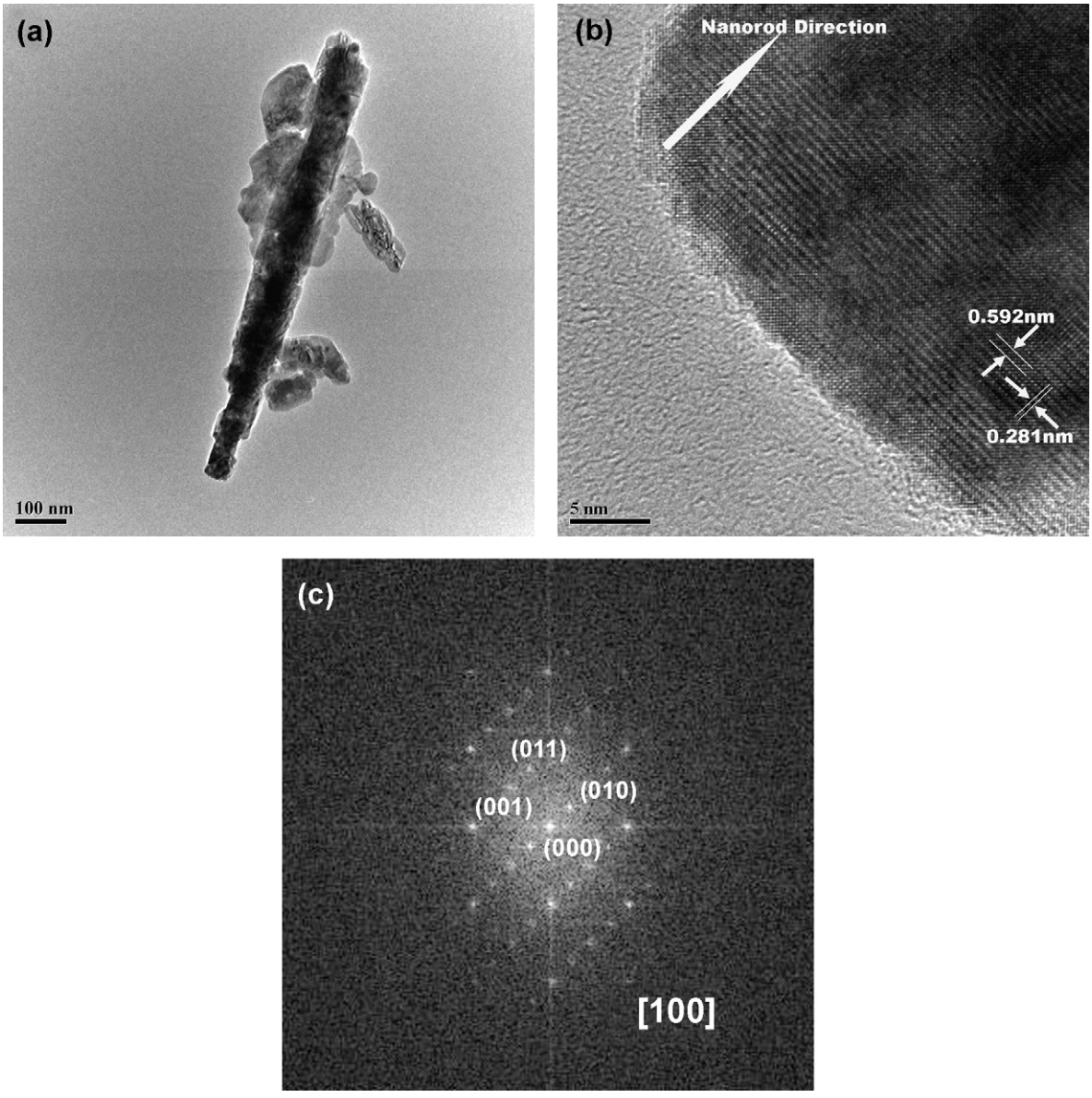

Fig. 4. TEM observation of $LiMnO_2$ nanorod, indicating a preferred growth along *b* axis. (a) A single nanorod, (b) HRTEM of the nanorod, showing the single crystal nature and preferred growth, and (c) FFT image of HRTEM, revealing an electron diffraction along [1 0 0] zone axis.

was observed. The detailed indexation of the diffraction pattern showed a orthorhombic structure for $LiMnO_2$ nanorod, with [1 0 0] zone axis. Furthermore, the nanorod direction (shown in Fig. 4b) was observed to parallel to 0 1 0 direction, implying that the nanorod has a preferred growth along *b* axis.

3.4. Electrochemical behavior of the nanorod o-$LiMnO_2$

The Li/o-$LiMnO_2$ cells were tested at current densities of 1/20*C* and 1/10*C* in the range between 2.0 and 4.5 V at room temperature (25 °C), as shown in Fig. 5a. In the case of the current density of 1/20*C*, two plateau around 4.0 and 2.9 V appeared, which can be ascribed to the phase transition during the cycling from o-$LiMnO_2$ to spinel phase since the different plateau represents that Li intercalation on different sites, tetrahedral site and octahedral site in the cycled-induced spinel $LiMn_2O_4$. The length of the 4 V plateau is getting longer, while that of 2.9 V plateau is getting shorter in further cycling, showing the increase in the spinel phase with the increasing cycles. The change in the capacity is also observed. The capacity of the powder after the first cycle is estimated around 260 mAh g^{-1}. After three cycles, the capacity gradually increased almost to the theoretical capacity (280 mAh g^{-1}) and then decreased dramatically. After seven cycles, a very large capacity loss (86 mAh g^{-1}) was observed, as shown in Fig. 5b, left side. However, when the cell was cycled under a high current density, 1/10*C*, a stable electrochemical property was observed, as shown in Fig. 5a at the bottom. Both the plateau at 4 and 2.9 V are very stable, and the capacity loss after 11 cycles is very small (less than 15 mAh g^{-1}), a stable capacity around 150 mAh g^{-1} was obtained, as shown in Fig. 5b. The capacity we got by the so designed MnOOH routine is almost the same compared to the reports by the other researchers [18–21], and thus suggests potential application in the lithium ion battery industry. Further investigation on increasing the stability of the cathode during the cycling is going on and will reported later.

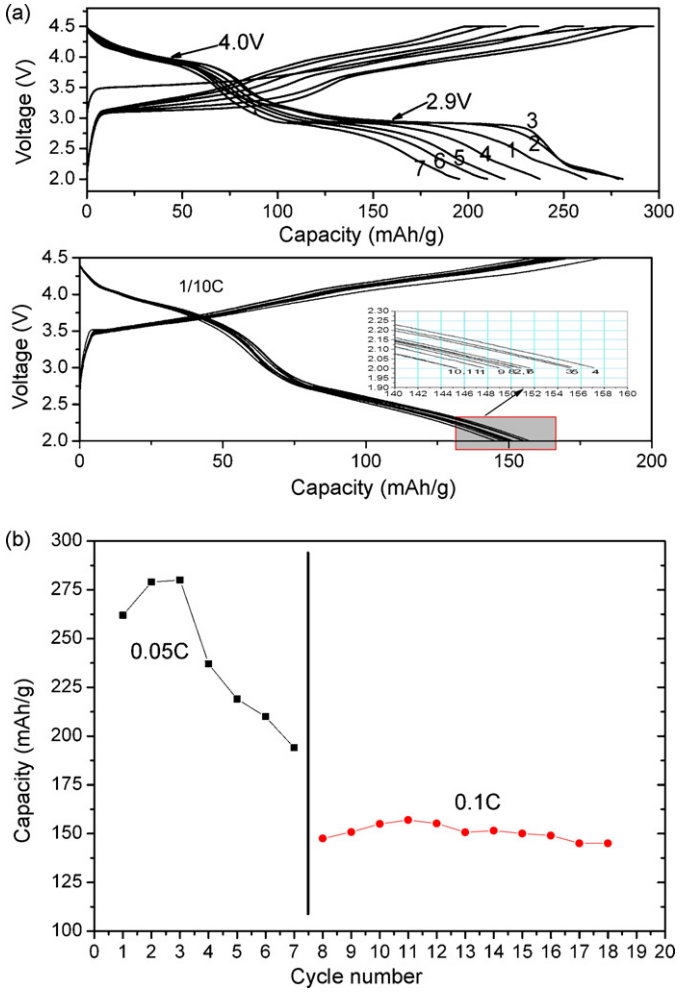

Fig. 5. Electrochemical properties of the prepared o-$LiMnO_2$ nanorod, showing high electric capacity and stable cyclability of the prepared cathode material. (a) Cycling curves of the Li/o-$LiMnO_2$ cells at current density of 1/20*C* and 1/10*C*, and (b) electric capacity of the o-$LiMnO_2$ cathode at different current density.

4. Conclusions

In summary, we demonstrated in the paper a hydrothermal routine for the preparation of orthorhombic $LiMnO_2$ nanorods for Li ion battery application. Phase conversion was observed during the Li ion incorporation process, in which several phases were identified as the intermediate phases. Morphological changes were also observed during the hydrothermal process, indicating that LiOH played two important role during the nanorod formation, one as the intercalating ion and the other as corrosive media. High resolution TEM observation revealed the single crystalline nature of the nanorods and a preferred growth direction along *b* axis direction was also determined. Nanorods prepared by such hydrothermal routine showed high electric capacity and stable cyclability at current density of 1/10*C*, showing potential application in the lithium ion battery field.

Acknowledgements

The research was financially supported from Shanghai Pujiang Project with project number 06PJ14048 and PRP project from Shanghai Jiaotong University with project number T05010014.

References

[1] A.R. Armstrong, P.G. Bruce, Nature 381 (1996) 499.
[2] K. Kang, Y.S. Meng, J. Breger, C.P. Grey, G. Ceder, Science 311 (2006) 977.
[3] R. Chitrakar, S. Kasaishi, A. Umeno, K. Sakane, N. Takagi, Y.S. Kim, K. Ooi, J. Solid State Chem. 169 (2002) 35.
[4] L. Croguennec, P. Deniard, R. Brec, J. Electrochem. Soc. 144 (10) (1997) 3323.
[5] Z.X. Shu, I.J. Davidson, R.S. McMillan, J.J. Murray, J. Power Sources 68 (1997) 618.
[6] J.N. Reimers, E.S. Fuller, E. Rossen, J.R. Dahn, J. Electrochem. Soc. 140 (12) (1993) 3396.
[7] M. Tabuchi, K. Ado, H. Kobayashi, H. Kageyama, Electrochem. Soc. Lett. 145 (1998) L49.
[8] F. Capitaine, P. Gravereau, C. Delmas, Solid State Ionics 89 (1996) 197.
[9] Y. Idemoto, T. Mochizuki, K. Ui, N. Koura, J. Electrochem. Soc. 153 (2) (2006) A418.

[10] R. Chitrakar, K. Sakane, A. Umeno, S. Kasaishi, N. Takagi, K. Ooi, J. Solid State Chem. 169 (2002) 66.
[11] J.M. Paulsen, C.L. Thomas, J.R. Dahn, J. Electrochem. Soc. 146 (10) (1999) 3560.
[12] R.J. Gummov, M.M. Thackeray, J. Electrochem. Soc. 141 (5) (1994) 1178.
[13] R. Chitrakar, H. Kanoh, Y. Miyai, K. Ooi, J. Solid State Chem. 163 (2002) 1.
[14] C.H. Lu, H.C. Wang, J. Eur. Ceram. Soc. 24 (2004) 717.
[15] X.Y. Tu, G.L. Lu, Y.W. Zeng, J. Mater. Sci. Technol. 22 (1) (2006) 45.
[16] T. Sakurai, T. Kimura, T. Sugihara, J. Power Sources 97/98 (2001) 366.
[17] X.Y. Tu, G.L. Lu, Y.W. Zeng, Z.Q. Yuan, X.R. Hu, J. Mater. Sci. Technol. 21 (4) (2005) 552.
[18] M.Q. Wu, Q.Y. Zhang, H.P. Lu, A. Chen, Solid State Ionics 169 (2004) 47.
[19] M.Q. Wu, A. Chen, R.Q. Xu, Y. Li, Microelectr. Eng. 66 (2003) 180.
[20] S. Komaba, S.T. Myung, N. Kumagai, T. Kanouchi, K. Oikawa, T. Kamiyama, Solid State Ionics 152/153 (2002) 311.
[21] S.T. Myung, S. Komaba, N. Kumagai, Electrochim. Acta 47 (2002) 3287.
[22] S.T. Myung, S. Komaba, N. Kumagai, J. Electrochem. Soc. 149 (10) (2002) A1349.
[23] S.T. Myung, S. Komaba, N. Kumagai, Chem. Lett. (2001) 80.
[24] G.H. Du, Z.Y. Yuan, G.V. Tendeloo, Appl. Phys. Lett. 86 (2005) 063113.
[25] Y.C. Zhang, T. Qiao, X.Y. Hu, W.D. Zhou, J. Cryst. Growth 280 (2005) 652.
[26] Y. Nitta, M. Nagayama, H. Miyake, A. Ohta, J. Power Sources 81/82 (1999) 49.
[27] G.R. Williams, A.J. Norquist, D. O'Hare, Chem. Mater. 18 (2006) 3801.
[28] S.T. Myung, A. Komaba, K. Kurihara, N. Kumagai, Solid State Ionics 177 (2006) 733.